JOURNAL OF SYNCHROTRON RADIATION

ISSN 1600-5775

Numerical study of the second harmonic generation in FELs

A. M. Kalitenko*

Department of Theoretical Physics, Faculty of Physics, M. V. Lomonosov Moscow State University, Moscow 119991, Russian Federation. *Correspondence e-mail: am.kalitenko@physics.msu.ru

Received 2 October 2020
Accepted 8 March 2021

Edited by M. Yabashi, RIKEN SPring-8 Center, Japan

Keywords: undulator; free-electron laser; computer simulation; second harmonic generation.

A numerical study of the effect of betatron oscillations on the second harmonic generation in free-electron lasers (FELs) is presented. Analytical expressions for the effective coupling strength factors are derived that clearly distinguish all contributions in subharmonics and each polarization of the radiation. A three-dimensional time-dependent numerical FEL code that takes into account the main FEL effects and the individual contribution of each electron to the second harmonic generation is presented. Also, the *X*- and *Y*-polarizations of the second harmonic are analyzed. The second harmonic was detected in experiments at the Advanced Photon Source (APS) Low Energy Undulator Test Line (LEUTL) and Linac Coherent Light Source (LCLS) in the soft X-ray regime. The approach presented in the article can be useful for a comprehensive study and diagnostics of XFELs. In the paper, the LCLS and Pohang Accelerator Laboratory X-ray Free-Electron Laser (PAL-XFEL) experiments are modeled. The simulation results are in a good agreement with the experimental data.

1. Introduction

In recent decades, the application of synchrotron radiation (Artcimovich & Pomeranchuk, 1945) as a free-electron laser (FEL) has been of increasing interest, largely due to the improved brightness of X-rays. As synchrotron radiation (Meinert *et al.*, 2010), FELs can be used to study various materials, crystals and nanostructures. Radiation in the FEL occurs due to the passage of an electron beam through a periodic magnetic structure called an undulator, where the interaction of electrons with radiation causes electrons to form microbunches where the electrons are spaced by the radiation wavelength (McNeil & Thompson, 2010; Pellegrini *et al.*, 2016; Huang & Kim, 2007).

The idea of an undulator, with the charges performing small transversal oscillations in a spatially periodic magnetic field and drifting at relativistic speeds along the undulator axis, was proposed by Ginzburg (1947). He also suggested that this radiation could be coherent if it were emitted from a series of electron bunches spaced by the radiation wavelength, with the bunch length being shorter than the radiation wavelength. Later in the mid-20th century, Motz *et al.* (1953) proposed an FEL amplifier consisting of a sequence of dipole magnets with alternating polarity and uniform spacing along the axis.

In 1971, Madey pointed out that, although the radiation of accelerated electrons differs from that of conventional lasers, the bremsstrahlung of electrons in a periodic magnetic field can be caused by application of an external radiation field (Madey, 1971). Since the electrons were not bound to atoms and molecules, Madey called this device the free-electron laser.

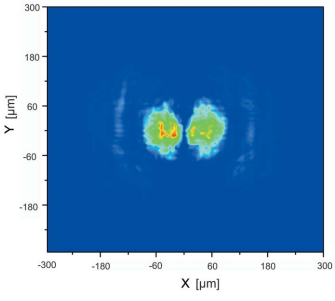

Single-pass high-gain FELs do not require optical resonators, so their spectrum is not limited by the reflective properties of the mirrors [see, for example, Uehara *et al.* (1984)].

In addition to the dominant fundamental harmonic, FEL radiation contains higher harmonics. However, due to the finite size of the electron beam and betatron oscillations, even harmonics can contribute to the FEL radiation, as was observed in experiments (Tremaine *et al.*, 2002; Biedron *et al.*, 2002; Ratner *et al.*, 2011). The strong focusing via the quadrupoles also causes betatron oscillation. In our simulations the effect of strong focusing on the second harmonic generation is also taken into account.

Second harmonic generation in crystals (Kleinman, 1962) is the main nonlinear optical effect. It is used to study the optical properties of new materials (Boursier *et al.*, 2015), and therefore it is desirable to take into account the power of the FEL second harmonics. Multi-harmonic radiation is also used for research purposes, especially if laser beams with different wavelengths can be obtained so that complete spatial overlapping is maintained even when both beams are focused to the diffraction-limited spot sizes. For example, higher-harmonic lasers can be used in two-photon spectroscopy (Kaiser & Garrett, 1961; Perrella *et al.*, 2013). The beam quality limits the number of harmonics that can effectively be generated at FELs, so even harmonics and their properties are important when designing lasers with multiple radiation harmonics.

In this paper, we derive new analytic expressions of the coupling factors for a planar undulator with consideration for averaged betatron oscillations. To study modern FELs in the X-ray range, various numerical programs are used [see the comparative analysis by Biedron *et al.* (2000)]. In some XFELs the second harmonic of a high power can be recorded. This paper presents a numerical study of the contribution from betatron oscillations to the second harmonic generation; the numerical modeling of harmonics is performed and their contribution to the generation of FEL radiation is estimated.

2. Undulator radiation in a planar single-frequency undulator with consideration of betatron oscillations

Let us consider the periodic field in the gap of a planar single-frequency undulator [see, for example, Scharlemann (1985)],

$$\mathbf{H} = H_0\big[0, \sin(k_\mathrm{u} z)\cosh(k_\mathrm{u} y), \cos(k_\mathrm{u} z)\sinh(k_\mathrm{u} y)\big]. \quad (1)$$

The laws of electron motion in the field of the magnet configuration (1) are

$$x(t) = -\frac{Kc}{\gamma\,\Omega_\mathrm{u}}\sin\Omega_\mathrm{u} t + \hat{\beta}_x\, ct, \quad (2)$$

$$y(t) = y(0)\cos\Omega_\beta t + \frac{\dot{y}(0)}{\Omega_\beta}\sin\Omega_\beta t, \quad (3)$$

where

$$\Omega_\mathrm{u} = ck_\mathrm{u}\,\bar{\beta}_z, \quad (4)$$

$$\bar{\beta}_z = 1 - \frac{1}{2\gamma^2}\left(1+\frac{K^2}{2}\right) - \frac{\hat{\beta}_x^2}{2} - \frac{y^2(0)}{4c^2}\,\Omega_\beta^2 - \frac{\dot{y}^2(0)}{4c^2}, \quad (5)$$

$$\Omega_\beta = \frac{K\Omega_\mathrm{u}}{\sqrt{2}\gamma} \quad (6)$$

and $\hat{\beta}_x$ is an average velocity in the direction x. Betatron oscillations result from both strong and weak focusing. The contribution from strong focusing via quadrupole sections to the second harmonic generation is taken into account via velocities $\dot{y}(0)$, $\hat{\beta}_x$.

The brightness is the energy radiated per solid angle per unit frequency interval by an undulator field and is calculated from the Lienard–Wiechert integral (Jackson, 1975),

$$\frac{\mathrm{d}^2 I}{\mathrm{d}\omega\,\mathrm{d}\Omega} = \frac{e^2\omega^2}{4\pi^2 c}\left|\int_0^\infty \big[\mathbf{n}\times(\mathbf{n}\times\boldsymbol{\beta})\big]\exp\Big[i\omega\Big(t-\frac{\mathbf{nr}}{c}\Big)\Big]\,\mathrm{d}t\right|^2, \quad (7)$$

where e is the electron charge, c is the speed of light in a vacuum, ω is the radiation frequency, $\mathbf{r}$ is the electron trajectory, β is the reduced electron velocity, and $\mathbf{n}$ is the observation unit vector, which can be written as

$$\mathbf{n} = \left(\theta\cos\varphi, \theta\sin\varphi, 1-\frac{1}{2}\theta^2\right), \quad (8)$$

where θ is the observation angle and φ is the azimuthal angle.

It can be easily shown that brightness can be expressed as

$$\frac{\mathrm{d}^2 I}{\mathrm{d}\omega\,\mathrm{d}\Omega} = \frac{e^2\omega^2 T^2}{4\pi^2 c}\left[\mathrm{sinc}\Big(\frac{\nu}{2}\Big)\right]^2 \sum_{n,\,m=-\infty}^{\infty}\big[|T_{n,m;\,x}|^2 + |T_{n,m;\,y}|^2\big], \quad (9)$$

$$\nu = 2\pi N\left[\frac{\omega}{\omega_\mathrm{res}(n,m)} - 1\right], \qquad T = \frac{N\lambda_\mathrm{u}}{c}. \quad (10)$$

The coupling factors are then

$$T_{n,m;\,x} = J_n\times\tilde{J}_m\theta\cos\varphi + \frac{K}{2\gamma}\big(J_{n+1} + J_{n-1}\big)\times\tilde{J}_m - J_n\times\tilde{J}_m\hat{\beta}_x, \quad (11)$$

$$T_{n,m;\,y} = J_n\times\tilde{J}_m\,\theta\sin\varphi + \frac{iy(0)}{2c}\Omega_\beta\big(\tilde{J}_{m-1} - \tilde{J}_{m+1}\big)\times J_n - \frac{\dot{y}(0)}{2c}\big(\tilde{J}_{m-1} + \tilde{J}_{m+1}\big)\times J_n, \quad (12)$$

with resonant frequencies

$$\omega_\mathrm{res} = \Big[2\gamma^2\big(n\Omega_\mathrm{u} + m\Omega_\beta\big)\Big] \Big/ \Big\{1 + (K^2/2) + (\gamma\theta)^2 - 2\gamma^2\theta\hat{\beta}_x\cos\varphi + (\gamma\hat{\beta}_x)^2 + \big[y^2(0)\,\gamma^2/(2c^2)\big]\Omega_\beta^2 + \big[\dot{y}^2(0)\,\gamma^2/(2c^2)\big]\Big\}. \quad (13)$$

For convenience, the following functions are introduced,

$$J_h(\omega) = \frac{1}{2\pi}\int_{-\pi}^{\pi}\mathrm{d}\alpha\ \exp\Big[i\Big(h\alpha + \xi_1\sin\alpha + \xi_2\sin 2\alpha + \tilde{\xi}_1\sin\alpha\Big)\Big], \quad (14)$$

$$\tilde{J}_m(\omega) = \frac{1}{2\pi}\int_{-\pi}^{\pi} \mathrm{d}\beta \;\exp\Big\{i\big[m\beta + \xi_3\cos\beta + \xi_4\sin\beta + (\xi_5+\xi_6)\sin 2\beta + \xi_7\cos 2\beta\big]\Big\}, \tag{15}$$

with the following arguments,

$$\xi_1 = \frac{K\omega}{\Omega_u\gamma}\,\theta\cos\varphi, \quad \xi_2 = \frac{K^2\omega}{8\gamma^2\Omega_u}, \quad \tilde{\xi}_1 = -\frac{K\hat{\beta}_x}{\gamma\Omega_u}\,\omega,$$
$$\xi_3 = -\theta\omega\sin\varphi\,\frac{y(0)}{c}, \quad \xi_4 = -\theta\omega\sin\varphi\,\frac{\dot{y}(0)}{c\Omega_\beta}, \tag{16}$$
$$\xi_5 = -\frac{y^2(0)\,\omega}{8c^2}\,\Omega_\beta, \quad \xi_6 = \frac{\dot{y}^2(0)\,\omega}{8\Omega_\beta c^2}, \quad \xi_7 = \frac{\dot{y}(0)\,y(0)\,\omega}{4c^2}.$$

In our case, the resonant frequencies split due to betatron oscillations, n is the number of the main harmonic, m is the number of the betatron oscillations (sub)harmonic. However, since the period and amplitude of betatron oscillations are small, the splitting in the radiation of odd harmonics $n = 1, 3, \ldots$ is not noticeable. Betatron oscillations can also contribute to the generation of even harmonics $n = 2, 4, \ldots$, Y-polarized radiation splits into several subharmonics $m = 0, \pm1, \ldots$. The contribution of Y-polarization is considered theoretically (Xie, 2002; Geloni *et al.*, 2007) in another formalism.

The main contribution to the generation of even harmonics is expressed by the term $(K/2\gamma)(J_{n+1} + J_{n-1}) \times \tilde{J}_m$. A similar argument in a different formalism with series expansion was derived by Reiche & Musumeci (2007); the Bessel coefficients for the second harmonic in Reiche (1999) equals $(K/2\gamma)(J_{n+1} + J_{n-1}) \times \tilde{J}_m$. However, a term $J_n \times \tilde{J}_m\hat{\beta}_x$ also gives a contribution. For the LCLS experiment, this contribution increases the coupling factor by about 30%, and the square of this coefficient by 70%. For odd harmonics, the term $J_n \times \tilde{J}_m\hat{\beta}_x$ can be neglected, but for even harmonics we cannot do this. The contribution to the generation of even harmonics caused by weak focusing is orders of magnitude smaller than the effect of strong focusing. The second harmonic in planar single-frequency undulators is the result of mixing wiggler oscillations with betatron motion caused by strong focusing.

3. Simulation of experiments

The second harmonic of FEL radiation was registered in several experiments, for example the Advanced Photon Source's (Biedron *et al.*, 2002) LCLS (Linac Coherent Light Source) in the soft X-ray regime (Ratner *et al.*, 2011). The evaluation of second harmonic generation was made in the modification of the numerical code *GENESIS1.3* (Reiche & Musumeci, 2007), but *GENESIS*'s coupling coefficients have a different form from the above formulas and do not consider Y-polarization.

We designed a numerical program for FEL simulation with consideration of the second harmonic in the modern C++ programming language using parallel programming. Our three-dimensional numerical code is based on a mathematical model that is also used in such codes as *GENESIS* (Reiche, 1999) and *GINGER* (Fawley, 2002). In the case of even harmonics, the coupling coefficient is different for each particle. It depends on the position and momentum, so the developed numerical code assigns each particle its own coupling coefficient.

For Y-polarized radiation, there is a split of the second harmonic at the betatron frequency $\Omega_\beta = K\Omega_u/\sqrt{2}\gamma$, and for modern lasers the split of the second harmonic occurs mainly into two subharmonics, which are considered as separate harmonics, see Fig. 1. Fig. 1 shows the splitting of the Y-polarized second harmonic into subharmonics $m = 0, \pm1, \ldots$. For X-polarized radiation of the first harmonic, the split also occurs, see Fig. 2. However, the power of the harmonic radiation is proportional to the square of the coupling coefficient $|T_n|^2$; in addition, the electron beam has a Gaussian distribution, and, therefore, the contribution is mainly given by the electrons in the center of the beam.

Simulation of the LCLS and PAL-XFEL experiments is presented below. The center of the electron beam is located on the undulator axis and has a Gaussian distribution in all simulations.

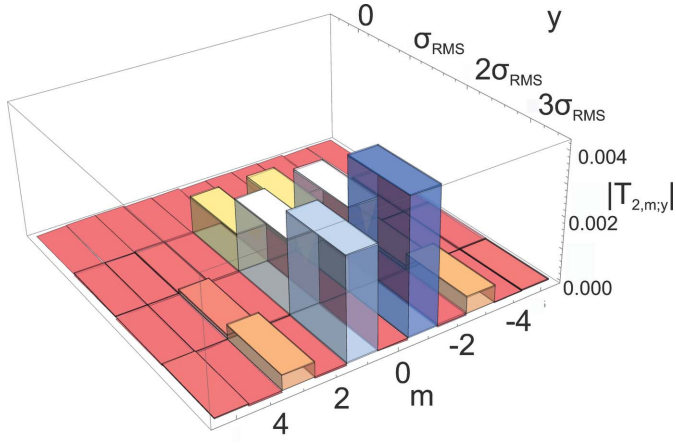

Figure 1
Split of the second harmonic (Y-polarization) in the LCLS experiment in the soft X-ray regime as a function of the distance y from the electron beam axis in units of root-mean-square beam size $\sigma_{\rm RMS}$.

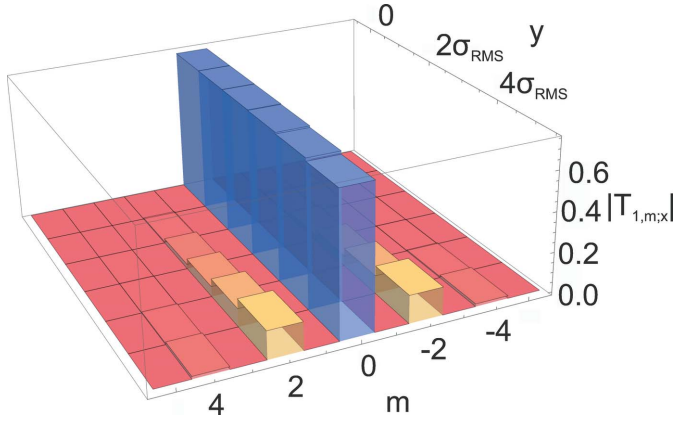

Figure 2
Split of the first harmonic (X-polarization) in the LCLS experiment in the soft X-ray regime as a function of the distance y from the electron beam axis in units of root-mean-square beam size $\sigma_{\rm RMS}$.

Table 1
Simulation parameters in the LCLS experiment in the soft X-ray regime used in the numerical program for FEL radiation.

The wavelength of the first harmonic $\lambda_1 = 1.5$ nm.

Undulator parameter	
K	3.5
Undulator period λ_u	3 cm
Number of periods in a section, N	114
Beam parameter	
Lorentz factor of electrons, γ	8400
Energy spread, σ_γ	0.03%
Emittance, ε_x	0.4 μm rad
Emittance, ε_y	0.4 μm rad
Peak current, I_0	1000 A

3.1. Simulation of the LCLS experiment in the soft X-ray regime

In the experiment (Ratner *et al.*, 2011) with XFEL LCLS (Emma *et al.*, 2010), higher harmonics were recorded, namely the second and third ones. In the soft X-ray experiment, the spatial distribution of the second harmonic intensity is also obtained. The wavelength of the first harmonic is 1.5 nm. Some relevant simulation data are collected in Table 1.

We estimated the radiation power of higher harmonics at the LCLS using the derived coupling coefficients, which are used in our three-dimensional program. Also, the second harmonic polarization analysis was performed. The Y-polarization of the second harmonic is caused by weak focusing in the undulator, and for the experiment (Ratner *et al.*, 2011) we estimate it at 3% of the second harmonic power. The results of numerical simulations give the following ratios between harmonic powers: for the third harmonic $P_3/P_1 \simeq 3\%$, for the fifth harmonic $P_5/P_1 \simeq 0.3\%$. It was mentioned by Ratner *et al.* (2011) that the fifth harmonic was not separated from the third one due to its small value, which simplified the study. The power ratio for the second harmonic is $P_2/P_1 \simeq 0.04\%$, which is within the experimental values of $P_3/P_1 \simeq 2.0$–2.5%, $P_2/P_1 \simeq 0.05$–0.06%. The lower power value for the third harmonic may be a consequence with the diffraction limit $\lambda_3/4\pi = 4 \times 10^{-11}$ m rad, and the emittance $\varepsilon = 4.8 \times 10^{-11}$ m rad, because by the end of saturation the emittance increases. However, an increase in the emittance leads to an increase in the power of the second harmonic. It should also be noted that the exact dynamics of electrons in the beam is unknown, so the power of the second harmonic was calculated based on experimental data.

Fig. 3 shows the evolution of the harmonic radiation power and electron bunching in the FEL in the self-amplified spontaneous emission (SASE) regime. The first harmonic $n = 1$ is represented by a black line, $n = 2$ by a red line, $n = 3$ by a blue line and $n = 5$ by a green line. The higher odd harmonics follow the principles of nonlinear growth (Huang & Kim, 2001). The second harmonic also has a nonlinear growth, but its generation also depends on the dynamics and position of each electron in the beam.

The spatial distribution of the second harmonic intensity is shown below in Fig. 4. The distribution has a double

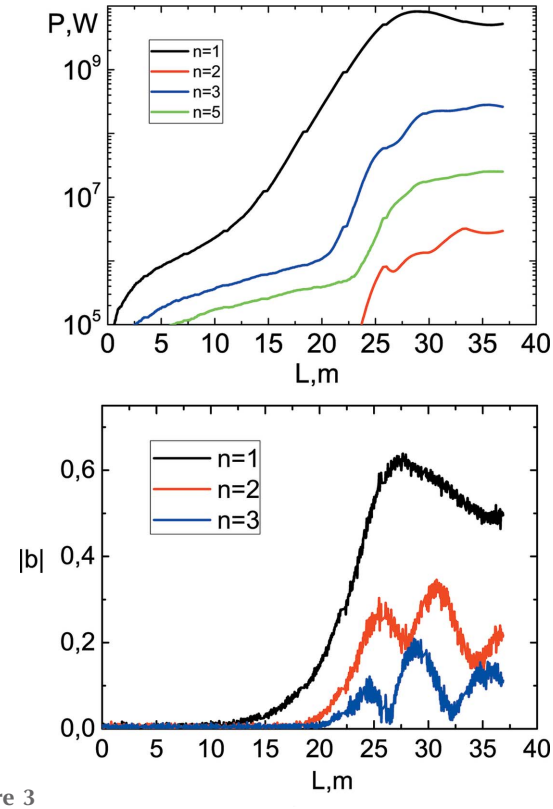

Figure 3
Simulation of the LCLS experiment in the soft X-ray regime using the author's program. Evolution of the harmonic power is shown at the top and the electron bunching coefficient is shown at the bottom. The harmonics are: $n = 1$, black line; $n = 2$, red; $n = 3$, blue; $n = 5$, green.

symmetric structure; some asymmetry is due to the beam asymmetry. Fig. 4 shows the X-polarization, which gives the prevailing contribution. In our simulations, we assume that the electrons in the beam have a Gaussian distribution.

We performed a comparative analysis of our program with *GENESIS* (Reiche, 1999) with the parameters of LCLS in the soft X-ray experiment. For clarity, we compared the harmonics

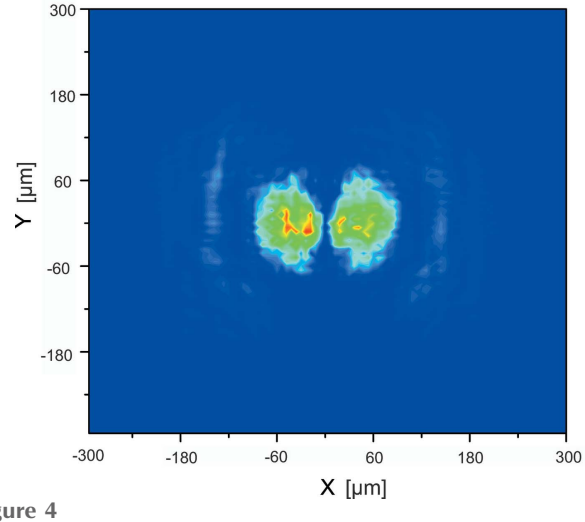

Figure 4
Spatial distribution of the X-polarization intensity of second harmonic radiation at the exit from the LCLS in the soft X-ray experiment.

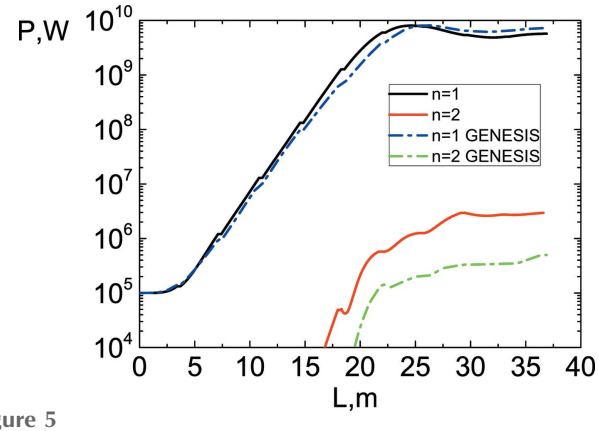

Figure 5
Comparison of the numerical program *GENESIS* and our program for the FEL amplifier with the experimental parameters of LCLS in the soft X-ray regime. Harmonics in our program (solid lines): $n = 1$, black; $n = 2$, red. Harmonics in *GENESIS* (dash-dotted lines): $n = 1$, blue; $n = 2$, green.

in the amplifier mode. As can be seen in Fig. 5, the fundamental harmonics of the radiation are almost exactly the same; the second harmonics differ by an order of magnitude. Our program estimates the second harmonic power at $P_2 = 2.9$ MW, the *GENESIS* estimate is 0.55 MW, and for the first harmonic we have $P_1 \simeq 8$ GW. We also compared the results in the SASE regime, with magnitudes and power ratios similar to Fig. 5. It should be noted that our program considers the interaction of electrons with radiation of the first and higher harmonics with numbers $n = 2, 3, 5$, which may be one of the reasons for the slightly accelerated growth of harmonics and a greater increase in the second harmonic power.

3.2. Simulation of the PAL-XFEL experiment in the soft X-ray regime

FEL experiments for soft and hard X-ray radiation were performed at the Pohang Accelerator Laboratory X-ray Free-electron Laser (PAL-XFEL); radiation with the fundamental harmonic wavelengths $\lambda = 1.52$ nm and $\lambda = 0.144$ nm was obtained. The experiments have been well documented; among other data, Kang *et al.* (2017) reported the evolution of harmonic power. We analyzed the generation of harmonics in the soft X-ray regime. Some relevant simulation data are collected in Table 2. The results are shown in Fig. 6 and discussed below.

PAL-XFEL as well as LCLS are FELs capable of generating radiation with a wavelength of the order of 1 Å. The undulator parameter $K = 2$ in the PAL-XFEL experiment was lower than that in the LCLS with $K = 3.5$, while the electron beam had a lower energy for the same generated wavelength. The soft X-ray radiation at $\lambda = 1.52$ nm was created by electrons with the energy $E = 3$ GeV; the energy spread in the simulation was set to $\sigma_e = 0.05\%$. The length of the undulator section is 5 m, the distance between the sections is 1 m, the undulator period is $\lambda_u = 3.4$ cm, and the parameter $K = 2$. Higher harmonics were not recorded in the experiment. A smaller undulator parameter K in PAL-XFEL, compared with in LCLS, results

Table 2
Simulation parameters of the PAL-XFEL experiment in the soft X-ray regime used in the numerical program for FEL radiation. The wavelength of the first harmonic $\lambda_1 = 1.52$ nm.

Undulator parameter	
K	2
Undulator period, λ_u	3.4 cm
Number of periods in a section, N	147
Beam parameter	
Lorentz factor of electrons, γ	5780
Energy spread, σ_γ	0.05%
Emittance, ε_x	0.55 μm rad
Emittance, ε_y	0.55 μm rad
Peak current, I_0	2200 A

in lower values of the coupling coefficients for odd higher harmonics.

We simulated the PAL-XFEL experiment using our numerical code. The evolution of harmonic power is presented in Fig. 6, the black line represents the first harmonic $n = 1$, red represents the second harmonic $n = 2$, and blue the third harmonic $n = 3$. The saturation power of the first harmonic is achieved at the length of ∼42 m as in the measurements (Kang *et al.*, 2017). The diffraction limit for a Gaussian photon beam with a wavelength of λ is $\varepsilon_r = \lambda/4\pi$. For the first harmonic, we have $\lambda_1/4\pi = 1.2 \times 10^{-10}$ m rad, and emittance $\varepsilon = 9.5 \times 10^{-11}$ m rad. The numerical program gives the following estimation for the power of the second and third

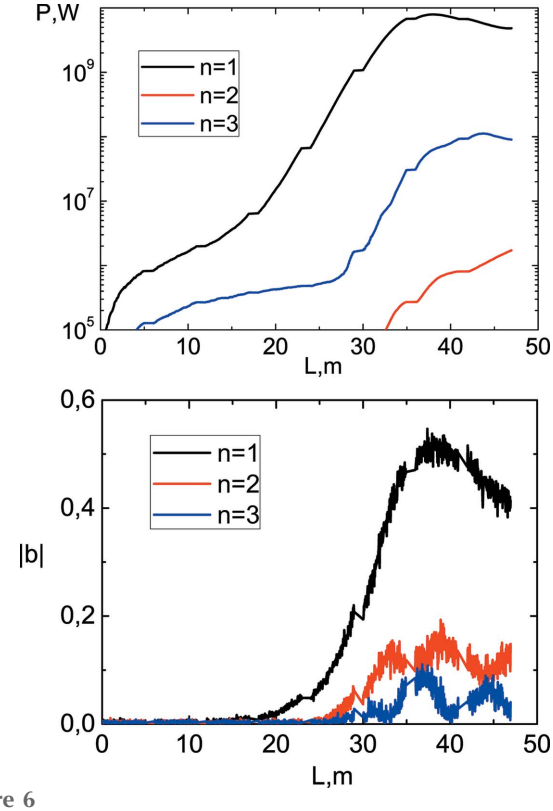

Figure 6
Simulation of the PAL-XFEL experiment in soft X-ray using the author's program. Evolution of the harmonic power is presented at the top; at the bottom the bunching coefficient. The harmonics are: $n = 1$, black line; $n = 2$, red; $n = 3$, blue.

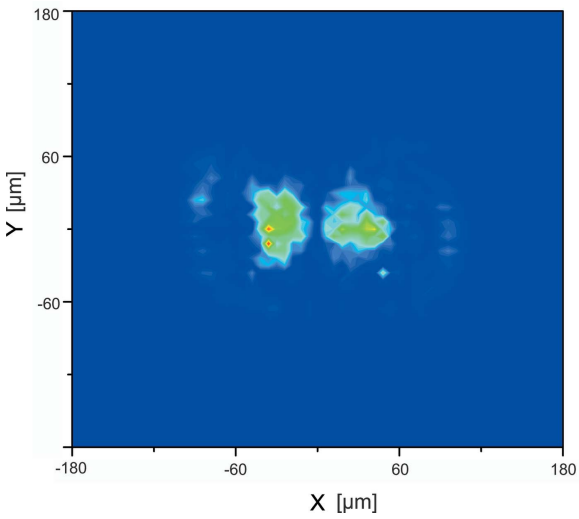

Figure 7
Spatial distribution of the X-polarization intensity of second harmonic radiation at the exit from the PAL-XFEL in the soft X-ray regime.

harmonics: the power ratio $P_2/P_1 \simeq 0.2\%$, the Y-component of the radiation of the second harmonic is $\sim$6.5%; for the third harmonic we have $P_3/P_1 \simeq 1.1\%$, the diffraction limit is not satisfied, so we should expect a decrease in the radiation power of higher harmonics. As can be seen, the third harmonic is relatively weaker than in the LCLS experiment, since the undulator parameter is smaller, which leads to lower coupling coefficients. The second harmonic also has a smaller relative contribution to radiation compared with the LCLS experiment. In Fig. 6 the bottom graph is the evolution of bunching – the bunching coefficient for the second and third harmonics is relatively smaller than at the LCLS. The spatial density of the second harmonic distribution, for X-polarization, is shown in Fig. 7 – it also has a double lobe structure.

4. Conclusions and discusions

We have obtained analytic expressions for the coupling factors in a planar undulator, taking into account betatron oscillations. These factors differ from those of Reiche & Musumeci (2007) by another term, which increases the discussed coupling factors by $\sim$30%. This allows the power of even harmonics to be calculated more precisely. We have written a program that simulates the generation of harmonics with n = 1, 2, 3, 5 harmonic numbers, and for the second harmonic the contribution of Y-polarization is considered.

The obtained rigorous theoretical results can be used to study radiation in FELs operating in a wide range of wavelengths, from infrared to X-ray. We studied an experiment with LCLS in the soft X-ray region (Ratner *et al.*, 2011), in which the second and third harmonics of radiation were registered. We compared our results with the *GENESIS* simulation, which showed that in our program the second harmonic has a greater contribution to radiation. Our numerical program with integrated derived analytical expressions gives the result $P_2/P_1 \simeq 0.04\%$, which indicates a good agreement with the experiment. We also analyzed the generation of higher harmonics at the PAL-XFEL (Kang *et al.*, 2017) experiment at the POHANG laboratory. We suppose that the higher harmonics should be weaker than at LCLS due to the smaller undulator parameter K. We have demonstrated a possible theoretical emission of harmonics at PAL-XFEL, but the beam parameters hardly allow us to expect the detection of harmonics above the third one. In experiments, the spatial power distributions of the second harmonic were obtained, Figs. 4 and 7. They have a double lobe structure, as was recorded by Ratner *et al.* (2011). Our formalism can also be applied to other magnetic field configurations, for example for asymmetric elliptic undulators (Kalitenko & Zhukovskii, 2020) and two-frequency undulators (Zhukovsky & Kalitenko, 2019).

The results obtained using the theoretical formalism and numerical code developed by us are consistent with the experiments and refine the previous expressions for the coupling factors of even harmonics. The presented formalism makes it possible to carry out more precise current and planned FEL experiments for examination of new materials, nanostructures, and to evaluate the efficiency, spectrum and harmonic generation at existing and constructed FELs, for example (Owada *et al.*, 2020).

APPENDIX *A*
Simulation parameters in the experiments

This section provides an overview of the simulation parameters of the experiments presented in the article. The simulations start in the center of the first quadrupole, which simplifies the matching of the electron beam (α_x, α_y = 0). See Table 3 and Table 4.

Table 3
Simulation parameters in the LCLS experiment in the soft X-ray regime used in the numerical program for FEL radiation.

Undulator parameters	
K	3.5
Undulator period, λ_u	3 cm
Number of periods in a section, N	114
Number of sections	10
Beam parameters	
Lorentz factor of electrons, γ	8400
Energy spread, σ_γ	0.03%
Emittance, ε_x	0.4 μm rad
Emittance, ε_y	0.4 μm rad
Averaged beta function, $\langle\beta_x\rangle$	10 m
Averaged beta function, $\langle\beta_y\rangle$	10 m
Peak current, I_0	1000 A
Focusing parameters	
Quadrupole focusing strength, g	40 T m^{-1}
Quadrupole length, QL	10 cm
Length of FODO cell, L_{FODO}	7.44 m
Other parameters	
Number of macroparticles in a slice, N_{slice}	6400
Mesh size	3 μm
Radiation wavelength of the first harmonic, λ_1	1.52 nm
Integration step length	3 cm
Separation of beam slices (in λ_1)	1

Table 4
Simulation parameters in the PAL-XFEL experiment in the soft X-ray regime used in the numerical program for FEL radiation.

Undulator parameters	
K	2
Undulator period, λ_u	3.4 cm
Number of periods in a section, N	147
Number of sections	8
Beam parameters	
Lorentz factor of electrons γ	5780
Energy spread, σ_γ	0.05%
Emittance, ε_x	0.55 μm rad
Emittance, ε_y	0.55 μm rad
Averaged beta function, $\langle\beta_x\rangle$	20 m
Averaged beta function, $\langle\beta_y\rangle$	20 m
Peak current, I_0	2200 A
Focusing parameters	
Quadrupole focusing strength, g	12 T m^{-1}
Quadrupole length QL	10 cm
Length of FODO cell, L_{FODO}	12 m
Other parameters	
Number of macroparticles in a slice, N_{slice}	6400
Mesh size	6 μm
Radiation wavelength of the first harmonic, λ_1	1.52 nm
Integration step length	3.4 cm
Separation of beam slices (in λ_1)	1

In the manual by Kang *et al.* (2014) it was stated that the beta function can have a deviation of 73% in the soft X-ray regime; our estimates of the deviation of the beta function have the same order, but a smaller value, which satisfies the experimental data.

Acknowledgements

The author is grateful to Docent P. I. Pronin, Professor A. V. Borisov and Professor V. Ch. Zhukovsky for useful discussions.

Funding information

Funding for this research was provided by: Theoretical Physics and Mathematics Advancement Foundation 'BASIS' (grant No. 19-2-6-82-1).

References

Artcimovich, A. L. & Pomeranchuk, I. J. (1945). *J. Phys. USSR*, **9**, 267.
Biedron, S. G., Chae, Y. C., Dejus, R. J., Faatz, B., Freund, H. P., Milton, S. V., Nuhn, H.-D. & Reiche, S. (2000). *Nucl. Instrum. Methods Phys. Res. A*, **445**, 110–115.
Biedron, S. G., Dejus, R. J., Huang, Z., Milton, S. V., Sajaev, V., Berg, W., Borland, M., Den Hartog, P. K., Erdmann, M., Fawley, W. M., Freund, H. P., Gluskin, E., Kim, K. J., Lewellen, J. W., Li, Y., Lumpkin, A. H., Moog, E. R., Nassiri, A., Wiemerslage, G. & Yang, B. X. L. (2002). *Nucl. Instrum. Methods Phys. Res. A*, **483**, 94–100.
Boursier, E., Segonds, P., Debray, J., Inácio, P. L., Panyutin, V., Badikov, V., Badikov, D., Petrov, V. & Boulanger, B. (2015). *Opt. Lett.* **40**, 4591–4594.
Emma, P., Akre, R., Arthur, J., Bionta, R., Bostedt, C., Bozek, J., Brachmann, A., Bucksbaum, P., Coffee, R., Decker, F.-J., Ding, Y., Dowell, D., Edstrom, S., Fisher, A., Frisch, J., Gilevich, S., Hastings, J., Hays, G., Hering, Ph., Huang, Z., Iverson, R., Loos, H., Messerschmidt, M., Miahnahri, A., Moeller, S., Nuhn, H.-D., Pile, G., Ratner, D., Rzepiela, J., Schultz, D., Smith, T., Stefan, P., Tompkins, H., Turner, J., Welch, J., White, W., Wu, J., Yocky, G. & Galayda, J. (2010). *Nat. Photon.* **4**, 641–647.
Fawley, W. M. (2002). *Phys. Rev. ST Accel. Beams*, **5**, 070701.
Geloni, G., Saldin, E., Schneidmiller, E. & Yurkov, M. (2007). *Opt. Commun.* **271**, 207–218.
Ginzburg, V. L. (1947). *Izv. Acad. Sci. USSR (Phys.)*, **11**, 1651.
Huang, Z. & Kim, K.-J. (2001). *Nucl. Instrum. Methods Phys. Res. A*, **475**, 112–117.
Huang, Z. & Kim, K.-J. (2007). *Phys. Rev. ST Accel. Beams*, **10**, 034801.
Jackson, J. D. (1975). *Classical Electrodynamics.* New York: Wiley.
Kaiser, W. & Garrett, C. G. B. (1961). *Phys. Rev. Lett.* **7**, 229–231.
Kalitenko, A. M. & Zhukovskii, K. V. (2020). *J. Exp. Theor. Phys.* **130**, 327–337.
Kang, H., Min, C., Heo, H., Kim, C., Yang, H., Kim, G., Nam, I., Baek, S. Y., Choi, H., Mun, G., Park, B. R., Suh, Y. J., Shin, D. C., Hu, J., Hong, J., Jung, S., Kim, S., Kim, K., Na, D., Park, S. S., Park, Y. J., Han, J., Jung, Y. G., Jeong, S. H., Lee, H. G., Lee, S., Lee, S., Lee, W., Oh, B., Suh, H. S., Parc, Y. W., Park, S., Kim, M. H., Jung, N., Kim, Y., Lee, M., Lee, B., Sung, C., Mok, I., Yang, J., Lee, C., Shin, H., Kim, J. H., Kim, Y., Lee, J. H., Park, S., Kim, J., Park, J., Eom, I., Rah, S., Kim, S., Nam, K. H., Park, J., Park, J., Kim, S., Kwon, S., Park, S. H., Kim, K. S., Hyun, H., Kim, S. N., Kim, S., Hwang, S., Kim, M. J., Lim, C., Yu, C., Kim, B., Kang, T., Kim, K., Kim, S., Lee, H., Lee, H., Park, K., Koo, T., Kim, D. & Ko, I. S. (2017). *Nat. Photon.* **11**, 708–713.
Kang, H.-S., Kim, D. E. & Ko, I. S. (2014). *PAL-XFEL Technical Design Report.* Pohang Accelerator Laboratory, Pohang, South Korea.
Kleinman, D. A. (1962). *Phys. Rev.* **126**, 1977–1979.
Madey, J. M. J. (1971). *J. Appl. Phys.* **42**, 1906–1913.
McNeil, B. W. J. & Thompson, N. R. (2010). *Nat. Photon.* **4**, 814–821.
Meinert, C., Filippi, J., Nahon, L., Hoffmann, S. V., D'Hendecourt, L., De Marcellus, P., Bredehöft, J. H., Thiemann, W. H. & Meierhenrich, U. J. (2010). *Symmetry*, **2**, 1055–1080.
Motz, H., Thon, W. & Whitehurst, R. N. J. (1953). *J. Appl. Phys.* **24**, 826–833.
Owada, S., Fushitani, M., Matsuda, A., Fujise, H., Sasaki, Y., Hikosaka, Y., Hishikawa, A. & Yabashi, M. (2020). *J. Synchrotron Rad.* **27**, 1362–1365.
Pellegrini, C., Marinelli, A. & Reiche, S. (2016). *Rev. Mod. Phys.* **88**, 015006.
Perrella, C., Light, P. S., Anstie, J. D., Stace, T. M., Benabid, F. & Luiten, A. N. (2013). *Phys. Rev. A*, **87**, 013818.
Ratner, D., Brachmann, A., Decker, F. J., Ding, Y., Dowell, D., Emma, P., Fisher, A., Frisch, J., Gilevich, S., Huang, Z., Hering, P., Iverson, R., Krzywinski, J., Loos, H., Messerschmidt, M., Nuhn, H. D., Smith, T., Turner, J., Welch, J., White, W. & Wu, J. (2011). *Phys. Rev. ST Accel. Beams*, **14**, 060701.
Reiche, S. (1999). *Nucl. Instrum. Methods Phys. Res. A*, **429**, 243–248.
Reiche, S., Musumeci, P. & Goldammer, K. (2007). *Proceedings of the 22nd Particle Accelerator Conference (PAC07)*, 25–29 June 2007, Albuquerque, NM, USA, pp. 1269–1271. TUPMS038.
Scharlemann, E. T. (1985). *J. Appl. Phys.* **58**, 2154–2161.
Tremaine, A., Wang, X. J., Babzien, M., Ben-Zvi, I., Cornacchia, M., Nuhn, H.-D., Malone, R., Murokh, A., Pellegrini, C., Reiche, S., Rosenzweig, J. & Yakimenko, V. (2002). *Phys. Rev. Lett.* **88**, 204801.
Uehara, Y., Fujiwara, E., Yamanaka, M., Tsuchida, K., Fujita, J., Kato, Y., Sasaki, W. & Saito, S. (1984). *Opt. Lett.* **9**, 539–541.
Xie, M. (2002). *Nucl. Instrum. Methods Phys. Res. A*, **483**, 527–530.
Zhukovsky, K. & Kalitenko, A. (2019). *J. Synchrotron Rad.* **26**, 159–169.